

Layer number dependent optical properties of multilayer hexagonal BN epilayers

X. Z. Du, M. R. Uddin, J. Li, J. Y. Lin, and H. X. Jiang^{a)}

Department of Electrical and Computer Engineering, Texas Tech University, Lubbock, Texas 79409, USA

(Received 17 January 2017; accepted 12 February 2017; published online 28 February 2017)

Deep ultraviolet photoluminescence emission spectroscopy has been employed to probe the layer number dependent near band-edge transitions above 5 eV in multilayer hexagonal boron nitride (*h*-BN) epilayers grown by metal-organic chemical vapor deposition. Two emission lines near 5.30 and 5.47 eV were resolved at 10 K. These two emission lines share similar spectroscopic features, and their energy peak separation is nearly independent of the number of layers. The observed energy separation of ~ 172 meV coincides well with the in-plane phonon vibration mode, E_{2g} , having an energy of 1370 cm^{-1} (~ 172 meV). The results suggested that the emission line at ~ 5.30 eV and ~ 5.47 eV are a donor-acceptor-pair transition and its one E_{2g} phonon replica, respectively. When the number of layers decreases from 100 to 8, the emission peak positions (E_p) of both emission lines blueshifted monotonically, indicating the dimensionality effects on the optical properties of *h*-BN. The layer number dependence of E_p can be described by an empirical formula, which accounts for the variations of the energy bandgap and activation energies of impurities with the number of layers. The results revealed that the impurity activation energies and the carrier-phonon coupling strength increase as the dimensionality of *h*-BN scales from thick layer to monolayer, suggesting that it is more difficult to achieve conductivity control through doping in monolayer or few-layer *h*-BN than in thick *h*-BN. *Published by AIP Publishing.*

[<http://dx.doi.org/10.1063/1.4977425>]

Hexagonal boron nitride (*h*-BN) has been recently under intensive study due to its unique physical properties including a wide energy bandgap (~ 6.5 eV), layered structure, high optical emission efficiency, high chemical and temperature stability, large in-plane thermal conductivity, as well as large thermal neutron capture cross-section of the isotope boron-10.^{1–14} It is a promising material for deep ultraviolet (DUV) optoelectronics devices^{1–12} and neutron detectors.^{13–15} A comprehensive study of the properties of the optical transitions in *h*-BN epilayers grown under controlled conditions provides not only a better understanding of its optical properties, but also an input for approaches towards the improvement of material quality, elimination of undesired defects or impurities, and conductivity control.

There have been several studies on the optical transitions in *h*-BN. A series of free exciton (or quasi Frenkel exciton) transitions in *h*-BN above 5.77 eV has been observed in high crystalline quality bulk crystals of small size,^{16–18} from which a large exciton binding energy ($E_B \approx 0.7$ eV) has been deduced in agreement with calculation results.^{1–3,6} More recently, we have also employed photoluminescence (PL) spectroscopy to probe the nature of a widely observed impurity related transition near 4.1 eV as well as the quasi-donor-acceptor pair (*q*-DAP) transition near 5.3 eV in *h*-BN epilayers synthesized under varying ammonia flow rates.^{19,20} The results inferred that the 4.1 eV and 5.3 eV *q*-DAP emission lines are due to the transitions between the nitrogen vacancy shallow donors and deep acceptors with energy levels of about 2.3 and 1.1 eV, respectively.^{19,20} However,

the layer number dependent optical transitions in few-layer *h*-BN have not been previously studied.

In this work, a set of *h*-BN epilayers with the layer number varying from 8 to 100 were grown by metalorganic chemical vapor deposition (MOCVD) on sapphire substrates. The precursors for boron and nitrogen were triethylboron (TEB) and ammonia (NH_3), respectively. To calibrate the number of layers of *h*-BN which is defined as the layer thickness divided by the interlayer distance between *h*-BN sheets of 3.33 \AA , a thick *h*-BN epilayer of $\sim 0.5\text{ }\mu\text{m}$ was grown, and the thickness was directly determined via optical micrograph, from which the growth rate was derived. Based on the pre-determined growth rate, a set of samples with identical growth conditions but varying growth times were grown. AFM image scans over a $2\text{ }\mu\text{m} \times 2\text{ }\mu\text{m}$ area revealed that the surface roughness of these *h*-BN epilayers varied from ~ 0.1 nm to ~ 0.5 nm as the layer number increases from 10 to 100. The PL measurement system utilized in this study includes a frequency-quadruped Ti-sapphire laser providing a lasing wavelength of 197 nm, 76 MHz repetition rate, 100 fs pulse width, and an average optical power of ~ 1 mW, a monochromator (1.3 m), a microchannel plate photomultiplier tube, and a closed-cycle He refrigerator with the temperature range between 10–800 K.

Figure 1 shows a low temperature ($T = 10$ K) PL spectra of the set of *h*-BN epilayers with varying number of layers grown under identical growth conditions. The samples were placed side-by-side during the PL measurements. As shown in Fig. 1, two dominant emission lines are clearly resolved around 5.30 eV and 5.47 eV in the PL spectrum of the thick *h*-BN sample (the 100 layer sample). A significant feature

^{a)}hx.jiang@ttu.edu

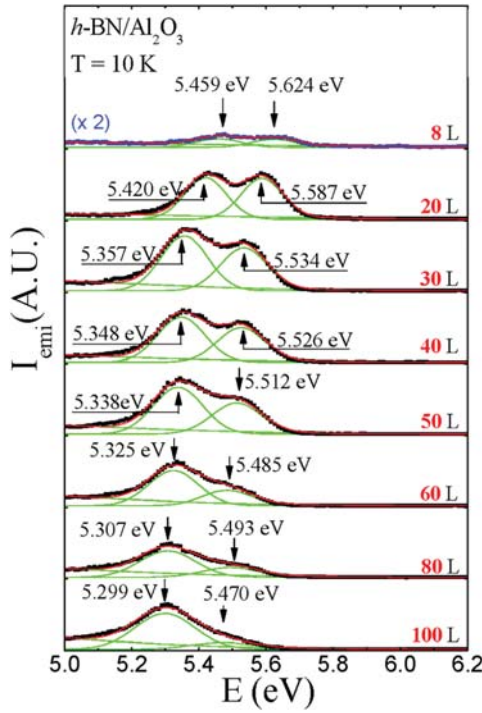


FIG. 1. 10 K PL spectra of h -BN epilayers with varying number of layers. The energy peak positions of the dominant emission lines are near ~ 5.30 and 5.47 eV in thick h -BN (epilayer with 100-layers).

shown in Fig. 1 is that both the emission lines exhibit a blue-shift towards higher energies when the number of layers is decreased from 100 to 8. The emission peaks (E_p) have been resolved using a multiple Gaussian fitting function. The evolutions of both emission peaks with the layer number are depicted in Fig. 2. As seen in Fig. 2(a), with an increase in the number of layers, both emission peak positions exhibit similar characteristics with an initial rapid decrease in energy followed by a slow decrease, and then eventually settled to constant values. The relationship between E_p and the layer number, $E_p(N)$, can be well described by the following equation:

$$E_p(N) = E_p(\infty) + [E_p(1) - E_p(\infty)] \exp(-(N-1)/B), \quad (1)$$

where $E_p(1)$, $E_p(N)$, and $E_p(\infty)$ denote, respectively, the emission peak positions of 1-layer, N -layer, and bulk h -BN, B is a fitting parameter which describes an exponential dependence of $E_p(N)$, and the quantity $[E_p(1) - E_p(\infty)]$ describes the total amount of energy peak shift as the dimensionality of h -BN scales from bulk to monolayer. Equation (1) reveals that the variation of the energy peak position with the h -BN layer number is a continuous and smooth function. From Eq. (1), the relationship between the observed energy peak position, $E_p(N)$, and layer number, N , can be obtained as

$$\frac{dE_p(N)}{dN} = -\frac{1}{B}E_p(N) + \frac{1}{B}E_p(\infty). \quad (2)$$

Equation (2) indicates that the change in the energy peak position, $E_p(N)$, depends on the h -BN layer number (N), which is expected. For instance, the change in E_p should be much larger when N is changing from 1 to 2 compared to that when N is changing from 100 to 101.

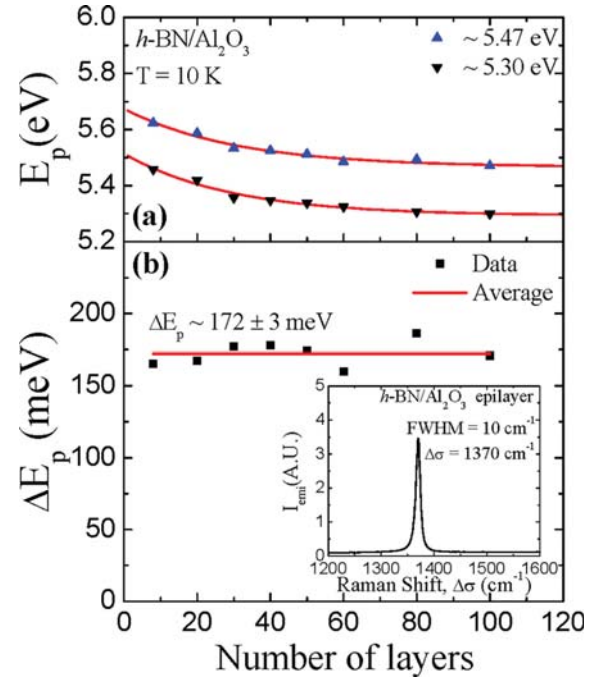


FIG. 2. (a) The layer number dependence of the energy peak positions of the dominant emission lines near 5.30 and 5.47 eV. The symbols are data points, and solid curves are the least squares fit with Eq. (1). The fitted values for the emission line around 5.30 eV are $E_p(1) = 5.506 \pm 0.010$ eV, $E_p(\infty) = 5.292 \pm 0.005$ eV, and $B = 29.6 \pm 5.3$ L. The fitted values for the emission line around 5.47 eV are $E_p(1) = 5.668 \pm 0.018$ eV, $E_p(\infty) = 5.466 \pm 0.013$ eV, and $B = 30.9 \pm 7.1$ L. (b) The energy peak separation between the two dominant emission lines (ΔE_p) as functions of the layer number measured at 10 K. The inset is a Raman spectrum of the reference $0.5 \mu\text{m}$ thick h -BN epilayer grown under identical conditions as those of the multi-layer h -BN with varying layer numbers.

As shown in Fig. 2, the equations for the peak position variations with N for the emission lines at ~ 5.30 and 5.47 eV follow:

$$E_{p,5.30\text{eV}}(N) = 5.292 \text{ eV} + (0.214 \text{ eV}) \times \exp(-(N-1)/(29.6 \pm 5.3)), \quad (3)$$

$$E_{p,5.47\text{eV}}(N) = 5.466 \text{ eV} + (0.204 \text{ eV}) \times \exp(-(N-1)/(30.9 \pm 7.1)). \quad (4)$$

The fittings provide the emission peak positions in bulk h -BN, $E_p(\infty)$, of ~ 5.292 and 5.466 eV, at 10 K. Since both emission lines have a relatively broad linewidth (>100 meV) and the peak positions are well below those of the free exciton transition series in bulk h -BN near 5.77 eV,^{16–18} these two emission lines are most likely related to the q -DAP and other impurity-related transitions. However, it is interesting to note that the variations of $E_p(N)$ with N for these two emission lines share nearly an identical spectroscopic feature. As shown in Fig. 2(b), the energy peak position difference between these two emission lines, $\Delta E_p = E_{p,5.47\text{eV}}(N) - E_{p,5.30\text{eV}}(N) \approx 172 \pm 3$ meV, is independent of N . In h -BN, it is well established that the in-plane phonon with E_{2g} vibration mode has an energy of 172 meV (1370 cm^{-1}).^{21,22} The inset of Fig. 2(b) shows a Raman spectrum of the reference h -BN epilayer grown under identical conditions with a thickness of $0.5 \mu\text{m}$. The observed Raman peak at

$\Delta\sigma = 1370 \text{ cm}^{-1}$ coincides well with the measured energy peak position difference between the two emission lines of 172 meV. Since this Raman peak is an in-plane mode, its energy depends very weakly on the layer number. It varies only $\sim 0.4 \text{ meV}$ from bulk to monolayer *h*-BN.²³ Based on these observations, we believe that one of these emission lines is most likely a phonon replica of the other. The emission line at $\sim 5.3 \text{ eV}$ has been identified to be a *q*-DAP transition in both bulk *h*-BN⁴ and thick *h*-BN epilayers.²⁰ Therefore we assign the emission lines at ~ 5.30 and 5.47 eV to the *q*-DAP transition and its one E_{2g} phonon replica, respectively.

It is interesting to note that a recent study has suggested that a transition between hexagonal BN to rhombohedral BN nitride could occur for films deposited on sapphire using CVD at a layer thickness of about 4 nm.²⁴ However, a separate study conducted on the growth of layered BN grown on sapphire by MOCVD has confirmed conclusively by cross-section STEM image of the stacking sequence of basal planes that the phase of thick BN films ($\sim 30 \text{ nm}$) is hexagonal rather than rhombohedral.²⁵ The observed smooth variation with the layer number of the PL emission peak positions shown in Fig. 2 suggests that an abrupt change in the bandgap of *h*-BN with varying layer numbers is absent, supporting the fact that MOCVD grown films retain the hexagonal phase as the layer number is increased.²⁵ It is possible that the observed rhombohedral phase BN is due to the use of different initial nucleation conditions.²⁴

As shown in Eq. (3), the emission peak at $\sim 5.30 \text{ eV}$ is blue shifted by $\sim 0.21 \text{ eV}$ from bulk to monolayer *h*-BN. However, the calculated energy bandgap, E_g , is expected to increase by $\sim 1.2 \text{ eV}$ from bulk to monolayer *h*-BN,³ which is much larger than the observed increase in the energy peak positions of the emission lines. By neglecting the Coulomb interaction between donors and acceptors, the energy peak position of the *q*-DAP transition can be described as $h\nu_{DAP} = E_g - E_D - E_A$, where E_D and E_A are the activation energies of the involved donor and acceptor, respectively. Our experimental results suggest that the values of E_D and E_A in *h*-BN also vary with its layer number. The Bohr radius a_B of shallow donors in a semiconductor can be expressed as

$$a_B = \left(\frac{\hbar^2}{\pi^2 m_e E_D} \right)^{1/2}, \quad (5)$$

where \hbar is the Plank constant, and m_e is the effective mass of electron in *h*-BN. The value of E_D for nitrogen vacancy (V_N) shallow donors involved in the *q*-DAP transition at $\sim 5.3 \text{ eV}$ in thick *h*-BN epilayers has been experimentally determined to be 99 meV.^{19,20} Using a value of $0.5m_0$ (where m_0 denotes the mass of free electron) for the effective mass of electron in *h*-BN based on experimental¹⁶ and calculation results,²⁶ we deduce $a_B \approx 25 \text{ \AA}$ in thick *h*-BN. In *h*-BN, the interlayer distance between *h*-BN sheets is 3.33 \AA . Thus the wavefunction around the shallow donor covers about 15 layers of *h*-BN if the total layer number is more than 15. However, for monolayer or few-layer *h*-BN, the electron wavefunction will be deformed particularly in the direction perpendicular to the plane of *h*-BN sheet. As a result, when the number of layers of *h*-BN is decreased from thick to few layers or

monolayer, several effects are expected: (1) the in-plane wavefunction overlap between carriers will be enhanced, and (2) the screening will be reduced and will become more anisotropic, especially in the direction of *c*-axis, as the relative permittivity, ϵ , approaches to 1 for monolayer *h*-BN. The enhanced in-plane overlap between carriers together with decreased screening will result in an increase of the donor activation energy, E_D . In principle, E_D will increase by a factor of 4 as the dimensionality of semiconductors scales from bulk to 2D,²⁷ which means that the estimated activation energy of the shallow donor in monolayer *h*-BN is 4 times the value in thick *h*-BN, $E_D^{2D} = 4 \times E_D^{3D}$ ($\sim 99 \text{ meV}$) $\approx 0.4 \text{ eV}$.

On the other hand, a previous theoretical study has indicated that the energy bandgap E_g will increase by $\sim 1.2 \text{ eV}$ as the dimensionality of *h*-BN scales from bulk to monolayer,³ i.e., $E_g \approx 6.5 + 1.2 = 7.7 \text{ eV}$ in monolayer *h*-BN. However, according to Eq. (3), the energy peak position of the *q*-DAP is 5.506 eV ($= 5.292 + 0.214 \text{ eV}$) in monolayer *h*-BN. From these data, the activation energy of the deep acceptor involved in the *q*-DAP transition in monolayer *h*-BN can thus be deduced via $E_A = E_g$ (7.7 eV) $- E_D$ (0.4 eV) $- h\nu_{DAP}$ (5.506 eV) $= 1.8 \text{ eV}$. With the determination of the energy bandgap and the activation energies of the involved shallow donor and deep acceptor, the energy level diagram of the *q*-DAP transition in monolayer *h*-BN can be constructed, as shown in Fig. 3(b). It is interesting to note that for the deep level acceptor involved in the *q*-DAP transition, its activation energy increases by ~ 1.6 times from 1.1 to 1.8 eV as the dimensionality of *h*-BN reduces from thick layer to monolayer. The increase is relatively small in comparison with a factor of 4 increase for the involved shallow donor.

Another significant feature exhibited in Fig. 1 is that the intensity ratio of the 5.47 eV emission line to that of the 5.30 eV emission line decreases monotonically with an increase in the layer number. The relative emission intensity between the main zero-phonon peak $n=0$ ($E_p \sim 5.30 \text{ eV}$) and the phonon replica peak $n=1$ ($E_p \sim 5.47 \text{ eV}$) depends on the carrier-phonon coupling strength, which is expressed by Huang–Rhys factor S .²⁸ At low temperatures, the emission intensity of the n th phonon replica I_n and the main zero-phonon emission line I_0 follows the relation of $I_n = I_0 \times \frac{S^n}{n!}$.²⁸ For the $n=1$ phonon replica emission line

$$S = I_1/I_0. \quad (6)$$

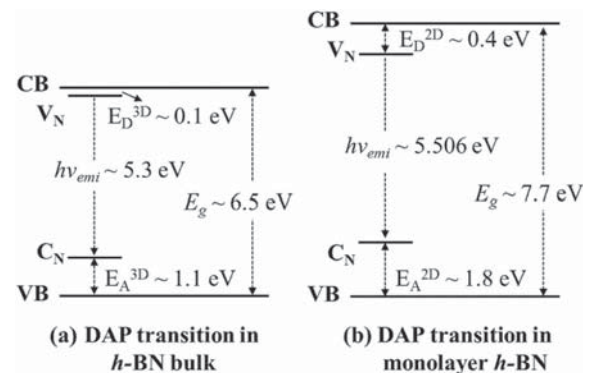


FIG. 3. Energy diagram of the DAP transition near 5.3 eV in (a) bulk *h*-BN and (b) monolayer *h*-BN.

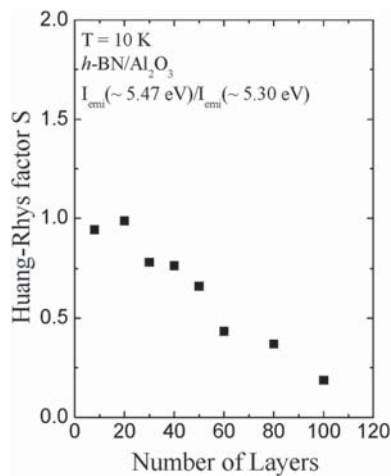


FIG. 4. The layer number dependence of the Huang–Rhys factor, S , in multilayer h -BN epilayers, measured at 10 K.

In Fig. 4, we plot the dependence of the Huang–Rhys factor S on the layer number. With an increase in the number of layers, the electron-phonon coupling strength is weakened. In other words, the carrier-phonon interaction in 2D is enhanced over that in 3D semiconductors, one of the well-known effects of reduced dimensionality in different material systems.

In summary, optical transitions related to a DAP recombination in multilayer h -BN have been studied via PL emission spectroscopy. Two emission lines near 5.30 and 5.47 eV were resolved at low temperatures in h -BN of 100 layers. Based on their spectroscopic characteristics as well as the fact that the energy difference between these two peaks (~ 172 meV) is almost independent of the number of layers, we attributed the emission line near 5.30 eV and 5.47 eV to a DAP transition and its one E_{2g} phonon replica, respectively. As the dimensionality of h -BN scales from thick layer to monolayer, the emission peak positions blue shifted by ~ 0.21 eV due to the increase of the energy bandgap, activation energies of shallow donors and deep acceptors. Moreover, the carrier-phonon interaction was significantly enhanced in monolayer and few-layers h -BN over that in thick h -BN. Our results suggest that compared to thick h -BN, it will be more difficult to achieve conductivity control through doping in monolayer or few layers h -BN due to the increases in the activation energies of impurities.

The effort on h -BN growth of h -BN is supported by ARO and monitored by Dr. Michael Gerhold (W911NF-16-1-0268) and the effort on the basic structural property

studies is supported by NSF (EECS-1402886). Jiang and Lin are grateful to the AT&T Foundation for the support of Ed Whitacre and Linda Whitacre endowed chairs.

- ¹B. Arnaud, S. Lebègue, P. Rabiller, and M. Alouani, *Phys. Rev. Lett.* **96**, 026402 (2006); **100**, 189702 (2008).
- ²L. Wirtz, A. Marini, M. Gruning, C. Attaccalite, G. Kresse, and A. Rubio, *Phys. Rev. Lett.* **100**, 189701 (2008).
- ³L. Wirtz, A. Marini, and A. Rubio, *Phys. Rev. Lett.* **96**, 126104 (2006).
- ⁴L. Museur and A. Kanaev, *J. Appl. Phys.* **103**, 103520 (2008).
- ⁵Y. Kubota, K. Watanabe, O. Tsuda, and T. Taniguchi, *Science* **317**, 932 (2007).
- ⁶B. Huang, X. K. Cao, H. X. Jiang, J. Y. Lin, and S. H. Wei, *Phys. Rev. B* **86**, 155202 (2012).
- ⁷K. Watanabe, T. Taniguchi, and H. Kanda, *Nat. Photonics* **3**, 591 (2009).
- ⁸R. Dahal, J. Li, S. Majety, B. N. Pantha, X. K. Cao, J. Y. Lin, and H. X. Jiang, *Appl. Phys. Lett.* **98**, 211110 (2011).
- ⁹S. Majety, X. K. Cao, J. Li, R. Dahal, J. Y. Lin, and H. X. Jiang, *Appl. Phys. Lett.* **101**, 051110 (2012).
- ¹⁰S. Majety, J. Li, X. K. Cao, R. Dahal, B. N. Pantha, J. Y. Lin, and H. X. Jiang, *Appl. Phys. Lett.* **100**, 061121 (2012).
- ¹¹J. Li, S. Majety, R. Dahal, W. P. Zhao, J. Y. Lin, and H. X. Jiang, *Appl. Phys. Lett.* **101**, 171112 (2012).
- ¹²X. Z. Du, C. D. Frye, J. H. Edgar, J. Y. Lin, and H. X. Jiang, *J. Appl. Phys.* **115**, 053503 (2014).
- ¹³J. Li, R. Dahal, S. Majety, J. Y. Lin, and H. X. Jiang, *Nucl. Instrum. Methods Phys. Res., Sect. A* **654**, 417 (2011).
- ¹⁴T. C. Doan, S. Majety, S. Grendadier, J. Li, J. Y. Lin, and H. X. Jiang, *Nucl. Instrum. Methods Phys. Res., Sect. A* **748**, 84 (2014).
- ¹⁵A. Maity, T. C. Doan, J. Li, J. Y. Lin, and H. X. Jiang, *Appl. Phys. Lett.* **109**, 072101 (2016).
- ¹⁶X. K. Cao, B. Clubine, J. H. Edgar, J. Y. Lin, and H. X. Jiang, *Appl. Phys. Lett.* **103**, 191106 (2013).
- ¹⁷K. Watanabe and T. Taniguchi, *Phys. Rev. B* **79**, 193104 (2009).
- ¹⁸L. Museur, G. Brasse, A. Pierret, S. Maine, B. Attal-Tretout, F. Ducastelle, A. Loiseau, J. Barjon, K. Watanabe, T. Taniguchi, and A. Kanaev, *Physica Status Solidi RRL* **5**, 214 (2011).
- ¹⁹X. Z. Du, J. Li, J. Y. Lin, and H. X. Jiang, *Appl. Phys. Lett.* **106**, 021110 (2015).
- ²⁰X. Z. Du, J. Li, J. Y. Lin, and H. X. Jiang, *Appl. Phys. Lett.* **108**, 052106 (2016).
- ²¹R. J. Nemanich, S. A. Solin, and R. M. Martin, *Phys. Rev. B* **23**, 6348 (1981).
- ²²R. V. Gorbachev, I. Riaz, R. R. Nair, R. Jalil, L. Britnell, B. D. Belle, E. W. Hill, K. S. Novoselov, K. Watanabe, T. Taniguchi, A. K. Geim, and P. Blake, *Small* **7**, 465 (2011).
- ²³L. H. Li, E. J. G. Santos, T. Xing, E. Cappelluti, R. Roldán, Y. Chen, K. Watanabe, and T. Taniguchi, *Nano Lett.* **15**, 218 (2015).
- ²⁴A. Henry, M. Chubarov, Z. Czigány, M. Garbrecht, and H. Högberg, *Jpn. J. Appl. Phys., Part 1* **55**, 05FD06 (2016).
- ²⁵X. Li, S. Sundaram, Y. E. Gmili, T. Ayari, R. Puybaret, G. Patriarche, P. L. Voss, J. P. Salvestrini, and A. Ougazzaden, *Cryst. Growth Des.* **16**, 3409 (2016).
- ²⁶Y. N. Xu and W. T. Ching, *Phys. Rev. B* **44**, 7787 (1991).
- ²⁷C. Weisbuch and B. Vinter, *Quantum Semiconductor Structures: Fundamentals and Applications* (Academic Press, San Diego, 2014), p. 25.
- ²⁸K. Huang and A. Rhys, *Proc. R. Soc. London, Ser. A* **204**, 406 (1950).